Ionics (2018) 24:577–587
DOI 10.1007/s11581-017-2202-y

ORIGINAL PAPER

Synthesis and electrochemical properties of rGO-MoS_2 heterostructures for highly sensitive nitrite detection

Jie Hu [1] · Jun Zhang [1] · Zhenting Zhao [1] · Jie Liu [1] · Jianfang Shi [1] · Gang Li [1] · Pengwei Li [1] · Wendong Zhang [1] · Kun Lian [1,2] · Serge Zhuiykov [3]

Received: 4 March 2017 / Accepted: 20 June 2017 / Published online: 1 July 2017

Abstract In this paper, the reduced graphene oxide (rGO) and molybdenum disulfide (MoS_2) (rGO-MoS_2) heterostructures have been successfully synthesized by a facile hydrothermal method. The crystal phase, surface morphology, and chemical composition of the obtained heterostructures were characterized by X-ray diffraction (XRD), scanning electron microscopy (SEM), transmission electron microscopy (TEM), and X-ray photoelectron spectroscopy (XPS) techniques. The electrochemical properties of the nitrite sensor attached with rGO-MoS_2 heterostructures were investigated using cyclic voltammetry (CV) and single-potential amperometry methods. The measured results show that the as-prepared sensor based on rGO-MoS_2/GCE exhibits a wide linear measurement range (0.2–4800 μM), low detection limit (0.17 μM), high sensitivity (0.46 μA μM^{-1} cm^{-2}), and good selectivity and reproducibility towards nitrite detection. The anti-interference property and real sample analysis were also investigated, which shows that the as-prepared rGO-MoS_2 heterostructures present great potential for practical applications.

Keywords Reduced graphene oxide · Molybdenum disulfide · Nitrite · Electrochemical sensor

Electronic supplementary material The online version of this article (doi:10.1007/s11581-017-2202-y) contains supplementary material, which is available to authorized users.

✉ Jie Hu
hujie@tyut.edu.cn

✉ Kun Lian
liankun@tyut.edu.cn

1 Micro and Nano System Research Center, Key Lab of Advanced Transducers and Intelligent Control System (Ministry of Education) and College of Information Engineering, Taiyuan University of Technology, Taiyuan, Shanxi 030024, China

2 School of Nano-Science and Nano-Engineering, Suzhou and Collaborative Innovation Center of Suzhou Nano Science and Technology, Xi'an Jiaotong University, Xi'an 710049, China

3 Department of Applied Analytical and Physical Chemistry, Faculty of Bioscience Engineering, Ghent University Global Campus, 119 Songdomunhwa-ro, Yeonsu-gu, Incheon 21985, South Korea

Introduction

In the past decades, great attentions have been attracted on determination and detection of nitrite (NO_2^-) because the high concentrations of nitrite can become poisonous to human beings and animals. Nitrite can form carcinogenic nitrosamines [1] and cause the loss of oxygen-carrying ability for hemoglobin in the human body [2]. Despite these facts, nitrite is widely used in the environment, beverages, and food products as a preservative [3], which has extensive existence in soil, natural water, and physiological systems [4]. In order to protect human health, the European Community has fixed the maximum limit of 0.1 mg L^{-1} (~2.2 mM) for nitrite in drinking water [5]. Therefore, it is necessary to accurately monitor nitrite in living environment and food technologies. Up to now, several analytical techniques such as spectrophotometry, flow injection analysis, chemiluminescence, and chromatography, have been developed for nitrite detection [6–10]. Among these methods, the electrochemical method is a simple, rapid, and low-cost methodology based on the oxidation or reduction of nitrite [11]. Moreover, the direct oxidation of nitrite on conventional electrode requires large overpotential. Hence, different kinds of electrochemical nitrite sensors have been developed based on the modified electrodes [12–14].

Recently, numerous two-dimensional (2D) nanostructured electrode materials, such as graphene, tungsten disulfide (WS_2), molybdenum disulfide (MoS_2), and conductive polymer materials have received considerable interests because of their intriguing quantum confined properties and excellent electrochemical performance [15–17]. Among all studied 2D nanostructures, graphene has been demonstrated to be one of the most promising electrode materials in electrochemical sensors owing to its good electrical conductivity, large contact surface area, strong mechanical strength, and a wide electrochemical window compared to the other 2D materials [18]. Moreover, graphene can be easily integrated with other 2D nanocrystals such as MoS_2, boron nitride (BN), or WS_2 to form heterostructures [19–21]. Among them, MoS_2, as a 2D layered structure, has attracted much attention in electrochemical terms due to its excellent electrocatalytic properties. For example, Huang et al. [22] reported the MoS_2 and chitosan-gold nanoparticle composites modified electrode as a novel electrochemical sensor constructed for the determination of bisphenol A (BPA). Chang et al. [23] synthesized the graphene-like MoS_2/amorphous carbon composites, exhibiting a high reversible capacity and excellent cyclic stability as anode materials for lithium ion batteries. Moreover, rGO-MoS_2 composites have been widely used in electrochemistry, such as reversible lithium storage, DNA detection, and supercapacitor [19, 24, 25]. Notably, Zhang et al. [26] demonstrated that a layered Mb/MoS_2–graphene/Nafion biosensor exhibited catalytic performance for the reduction of sodium nitrite ($NaNO_2$). However, its detection limit was poor and the direct reduction of NO_2^- on the layered MoS_2–graphene/Nafion was not investigated. Although considerable efforts have been devoted to the electrochemical applications of two-dimensional materials, to the best of our knowledge, seldom works have been conducted on rGO-MoS_2 heterostructures for nitrite detection.

In this work, the electrochemical sensor based on rGO-MoS_2 heterostructures has been developed for the nitrite detection. The microstructural characterization, elemental composition, and chemical state analysis of the rGO-MoS_2 heterostructures were analyzed through the different material characterization techniques. The electro-catalytic performances of as-fabricated sensor towards the nitrite detection were evaluated by cyclic voltammetry (CV) and single-potential amperometry. The results obtained have demonstrated that the as-prepared rGO-MoS_2/GCE sensor exhibits high sensitivity, low detection limit, wide linear concentration range, and high stability and availability for accurate NO_2^- detection.

Experimental

Chemicals and reagents

Graphite (325 meshes) was purchased from Qingdao Huatai Lubrication Sealing Technology Co. Ltd. Sodium molybdate ($Na_2MoO_4 \cdot 2H_2O$, >99.99%), thiourea (NH_2CSNH_2, ≥99.0%), and sodium nitrite ($NaNO_2$, ≥99.0%) were used from Sigma-Aldrich (Shanghai, China). Potassium permanganate ($KMnO_4$, >99.5%) was obtained from Sinopharm Chemical Reagent Co, Ltd. (Shanghai, China). All other reagents used in our experiments were of analytical reagent grade and were used without further purification. The deionized water (Milli-Q Millipore 18.2 MΩ cm resistivity) was used in all dilutions. The 0.1 M phosphate buffer solution (PBS) was prepared by mixing solutions of Na_2HPO_4 and NaH_2PO_4 and used as the supporting electrolyte.

Synthesis of the rGO-MoS_2 heterostructures

Graphene oxide (GO) was prepared by a modified Hummers method [27]. Firstly, 0.25 g of graphite and 0.25 g of $KMnO_4$ were mixed with 7.5 mL of H_2SO_4 (98%). Secondly, the mixture was stirred for 10 min at room temperature. Then, the reactants were kept at 50 °C and stirred for 3.5 h. After that, the mixture was diluted and the excess $KMnO_4$ removed by adding H_2O_2. Next, the mixed aqueous solution was washed with 10% HCl (36–38%). Subsequently, the precipitate was suspended in 150 mL of deionized water and underwent ultrasonic peeling for 1.5 h. Finally, the aqueous phase suspension of GO was obtained after centrifugation at 3500 rpm, and the concentration of GO solution was approximately 0.5 mg/mL.

The rGO-MoS_2 heterostructures were synthesized using a modified one-step hydrothermal method [28]. In a typical synthesis, 0.6 g $Na_2MoO_4 \cdot 2H_2O$ and 0.75 g NH_2CSNH_2 were dissolved into 30 mL GO suspension, and the solution was stirred for 20 min at room temperature. After that, the mixture was transferred into Teflon-lined autoclave and heated at 220 °C for 24 h. Then, the GO was reduced to the reduced graphene oxide (rGO). After cooling to room temperature, the black product was washed with DI water and anhydrous ethanol. Finally, the rGO-MoS_2 heterostructures were obtained by drying at 60 °C for 12 h.

Prior to modification, the surface of the GC electrode was polished to a mirror using 1.0 and 0.3 μm alumina particles, sonicated in ethanol and deionized water, and dried in air. Then, 2 mg as-prepared samples were dispersed into 1 mL deionized water to obtain homogeneous slurry (2 mg/mL). After that, a certain amount of rGO-MoS_2 slurry was dropped onto the surface of the GCE by pipette and dried at 60 °C for 1 h, which was defined as rGO-MoS_2/GCE. For comparison, rGO/GCE and MoS_2/GCE were prepared using the similar procedure. All of the modified electrodes were stored at 4 °C before use.

Characterization

XRD analysis was made on a MiniFlex II (Rigaku Corporation Cu-Kα1 radiation λ = 1.5406 Å) with a scanning speed of 3°/min. The morphology of as-synthesized hybrid structures was observed by scanning electron microscopy (SEM, JSM-7001F) with an accelerating voltage of 10 kV. The crystalline structures of the sample were further measured by transmission electron microscopy (TEM, JEM-2100F). The X-ray photoelectron spectroscopy (XPS, VG ESCALAB 250) measurements were performed on an Escalab 250Xi instrument with Mg-Kα radiation. All the electrochemical measurements were carried out on a Zahner IM6 electrochemical workstation with a conventional three-electrode system. A bare or modified GCE was used as the working electrode, and a Pt wire mesh electrode was used as the counter electrode. A silver chloride electrode (saturated KCl) was used as the reference electrode.

Results and discussion

Morphological and structural characterization

Figure 1 shows the XRD patterns of the as-synthesized rGO, MoS_2, and rGO-MoS_2 heterostructures, respectively. For rGO (Fig. 1a), the two peaks at about $2\theta = 24.40°$ and $2\theta = 42.85°$ can be assigned to the (002) and (100) planes of graphene sheets [29]. Compared with pure rGO, both MoS_2 and rGO-MoS_2 heterostructures exhibit the similar diffraction peaks corresponding to the (002), (100), (103), (110), which match well with the phase of MoS_2 (JCPDS 37-1492). Furthermore, it is worth noticing that the intensity of all the diffraction peaks of rGO-MoS_2 hybrid structures are much weaker than that of the pure MoS_2 structure, especially the (002) plane peaks, which suggests that the incorporation of the graphene

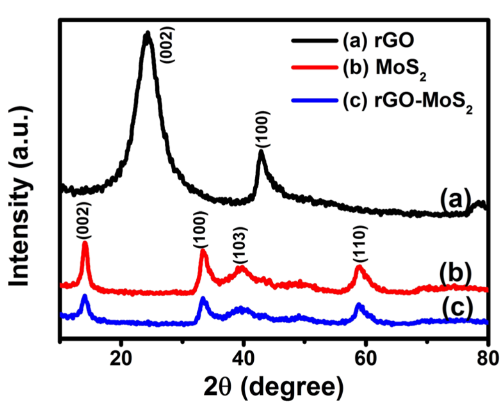

Fig. 1 XRD of the as-synthesized rGO (**a**), MoS_2 (**b**), and rGO-MoS_2 (**c**)

considerably inhibited the (002) plane growth of the MoS_2 crystals in the heterostructured composites [30].

The surface morphology and structure of the as-prepared rGO-MoS_2 samples were further characterized by SEM. Figure 2a depicts the SEM micrograph of the rGO and shows that the surface of the rGO has a wrinkled texture associated with the presence of the flexible and ultrathin graphene sheets. On the other hand, the morphology characterizations of the pure MoS_2 (Fig. 2b) revealed that the pristine MoS_2 nanoflakes tend to stack together tightly and exhibit a flower-like nanostructure. The thickness of petal-like nanoflakes is only about several nanometers. As a contrast, the rGO-MoS_2 heterostructures (Fig. 2c, d) exhibit the irregular three-dimensional nano-architecture. The drastic difference indicates the novel role of GO as an efficient substrate material for the growth of MoS_2, suppressing the stacking of MoS_2 nanoflakes [31]. The unique nano-architecture of rGO-MoS_2 can not only increase the surface contact area with the analytes but can also facilitate the rapid electronic transport of electrochemical reactions. Moreover, the developed rGO-MoS_2 heterostructures also possess an excellent stability due to the super strength of graphene.

To further study the morphology and the interplanar spacing of the synthesized rGO-MoS_2 heterostructures, TEM, HRTEM, and the corresponding selected-area electron diffraction (SAED) were performed on the as-synthesized rGO-MoS_2 heterostructures, as shown in Fig. 3. From the TEM images of rGO-MoS_2 (Fig. 3a, b), we can clearly observe that a large number of curved and wrinkled MoS_2 nanoflakes were dispersed on the surface of rGO, which was consistent well with the SEM image of rGO-MoS_2. Figure 3c exhibits the typical HRTEM image of rGO-MoS_2 heterostructures, and the measured interlayer distance is about 0.62 nm, which corresponds to the (002) lattice plane of MoS_2 [32]. Figure 3d illustrates the SAED pattern of the rGO-MoS_2 heterostructures, which is similar to the crystalline structure of pure MoS_2. The measured results unambiguously indicate that the stacking between the adjacent rGO sheets is suppressed due to the selective growth of MoS_2, which is consistent with the XRD results [31].

To determine the elemental composition and chemical state, XPS analysis was conducted on the rGO-MoS_2 heterostructures and the main results are illustrated in Fig. 4. The binding energies were calibrated to the C1s peak at 284.4 ± 0.1 eV of the surface adventitious carbon. It can be observed that only signals of Mo, S, C, and O elements present in the survey spectrum (Fig. 4a), which indicates the high purity of as-synthesized rGO-MoS_2 sample. Figure 4b displays the XPS profile of Mo 3d spectrum, which can be deconvoluted into three peaks. The measured two strong peaks with binding energy values of 229.4 and 232.5 eV can be

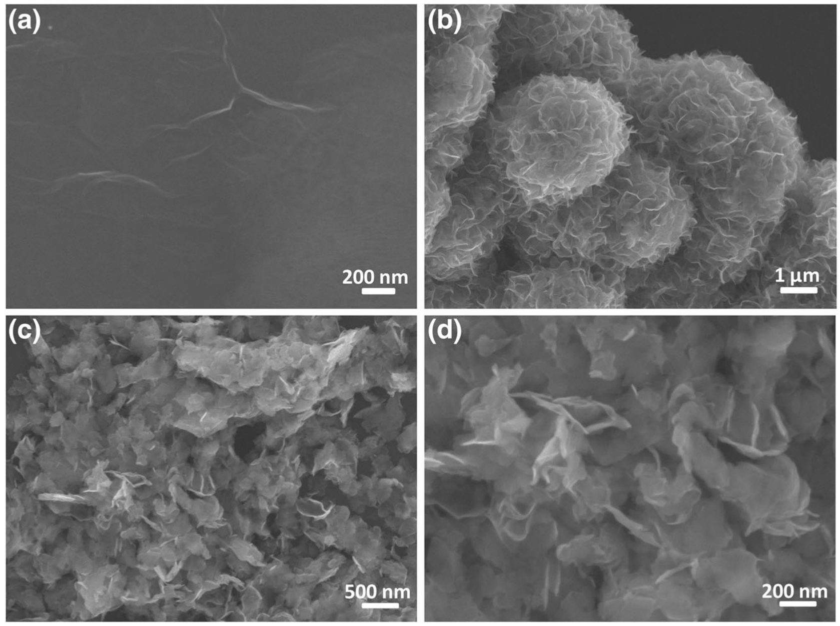

Fig. 2 Typical SEM images of the as-synthesized rGO (**a**), MoS_2 (**b**), and rGO-MoS_2 heterostructures (**c**, **d**)

assigned to the $Mo3d_{5/2}$ and $Mo3d_{3/2}$ peaks, respectively, while the weak peak is located at 226.4 eV is corresponding to S2s of MoS_2. Meanwhile, the S 2p spectrum shows two peaks at 162.2 eV and 163.4 eV (Fig. 4c), which could be attributed to the spin–orbit couple $S2p_{3/2}$ and $S2p_{1/2}$, respectively. These binding energies are all consistent with the previous reported values of MoS_2 crystal [33]. Figure 4d displays the spectrum of C1s, and the two peaks located at 284.6 and 286.8 eV can be ascribed to the C–C and C–O, respectively. Moreover, the low content of O suggests that GO has been adequately reduced to rGO by the solvothermal treatment.

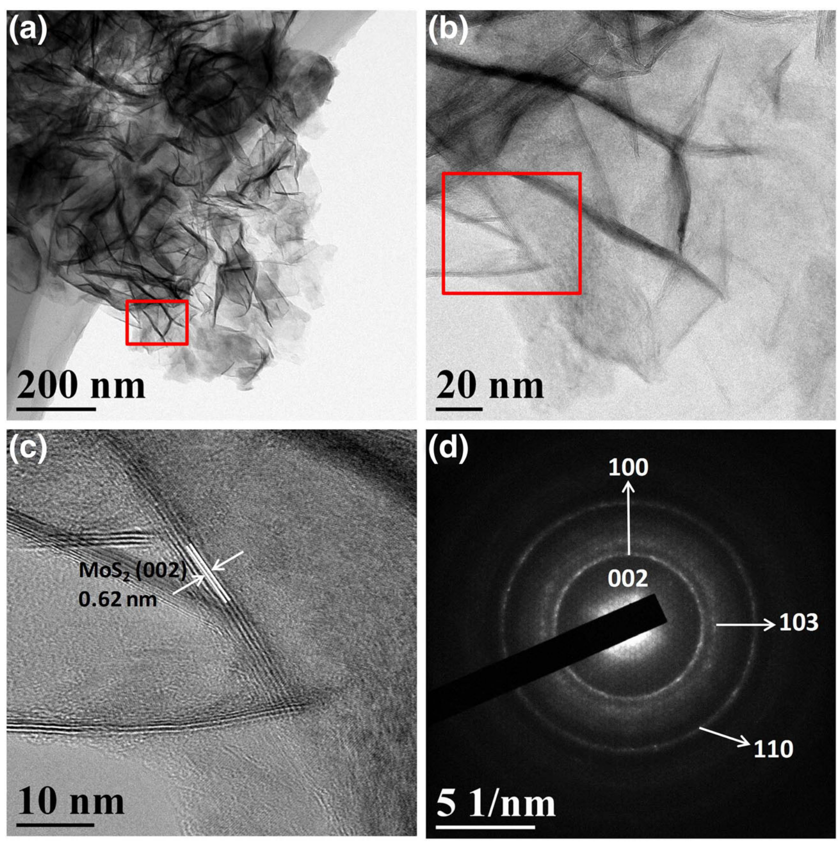

Fig. 3 **a** TEM image of rGO-MoS_2. **b**, **c** HRTEM images of rGO-MoS_2 (zoomed from the selected area in **a**, **b** respectively). **d** The corresponding SAED pattern

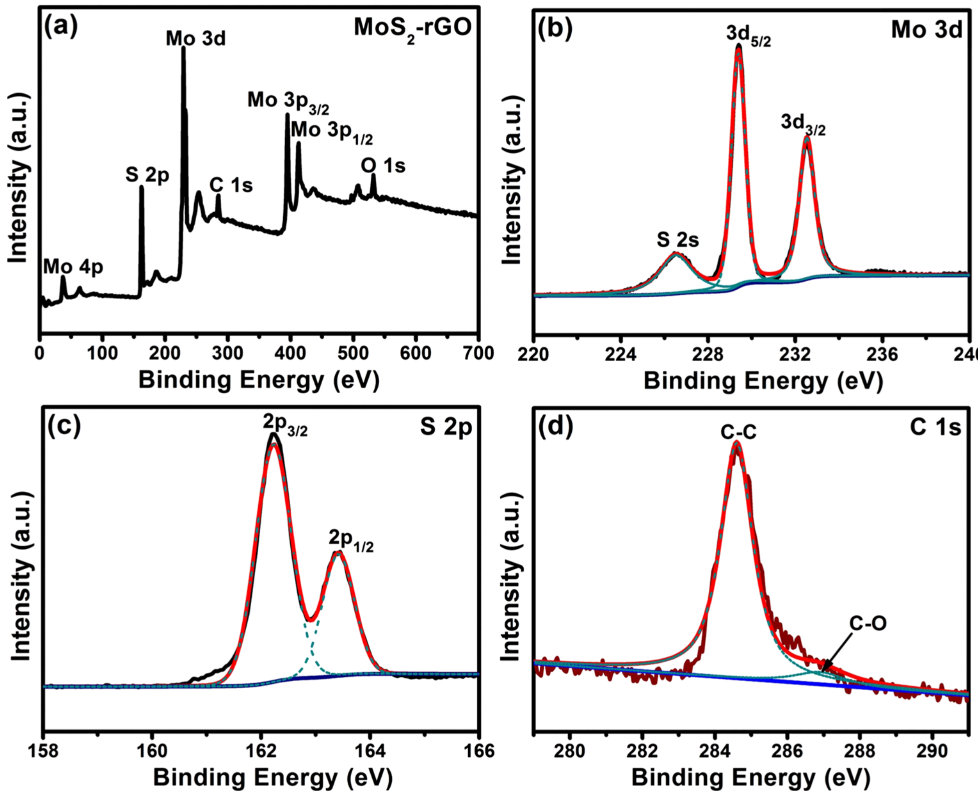

Fig. 4 XPS survey spectrum of rGO-MoS_2 heterostructures, **a** full survey scan spectrum, **b** Mo 3d, and **c** S2p and **d** C1s regions

Electrocatalytic oxidation of nitrite on electrodes

It is well known that the pH value can significantly influence the electrochemical performance of the electrochemical sensor. Here, the electrochemical response of rGO-MoS_2/GCE towards 500 μM nitrite was initially investigated by testing the CVs in the pH range of 6.0 to 8.0 in 0.1 M PBS. Figure 5a shows CV curves of rGO-MoS_2/GCE at different solution pH values in 500 μM nitrite. Clearly, the current response climbed up at first and reached to the maximum at pH 7.0, and then declined significantly with further increase of the pH value, as illustrated in Fig. 5b. Consequently, the pH 7.0 has been selected for the following experiments to obtain the high sensitivity.

The relationship between the peak current and modification amounts of rGO-MoS_2 were further investigated. Figure 6a shows the CV curves of rGO-MoS_2/GCE sensors towards 500 μM nitrite. The measured results reveal that the maximum peak current can reach to 45.3 μA, when the modification rGO-MoS_2 slurry is about 25 μL, as shown in Fig. 6b. The highest peak current can be ascribed to the reasons as follows: when a small amount of rGO-MoS_2 slurry was coated on the

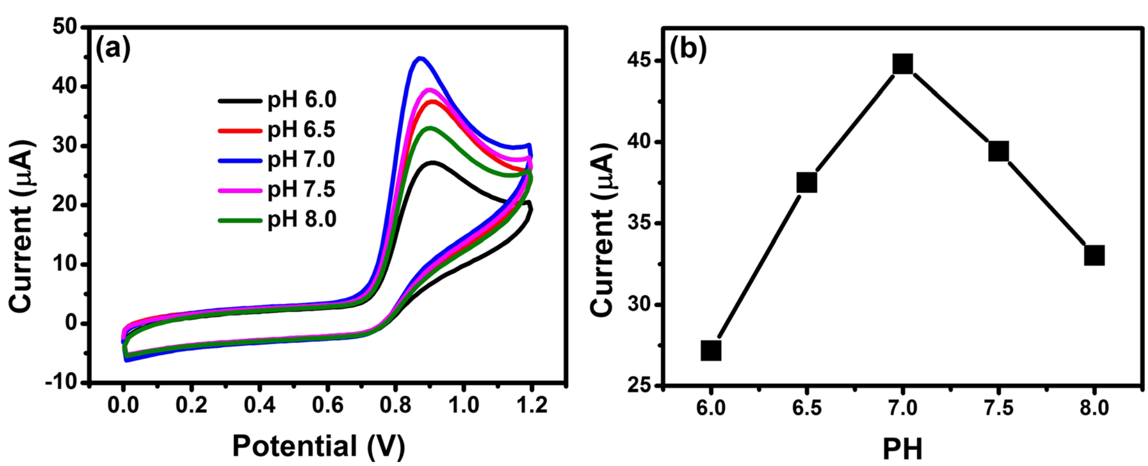

Fig. 5 **a** CV curves of rGO-MoS_2/GCE at different solution pH values in 500 μM nitrite. **b** Effect of different solution pH values on peak current in 500 μM nitrite

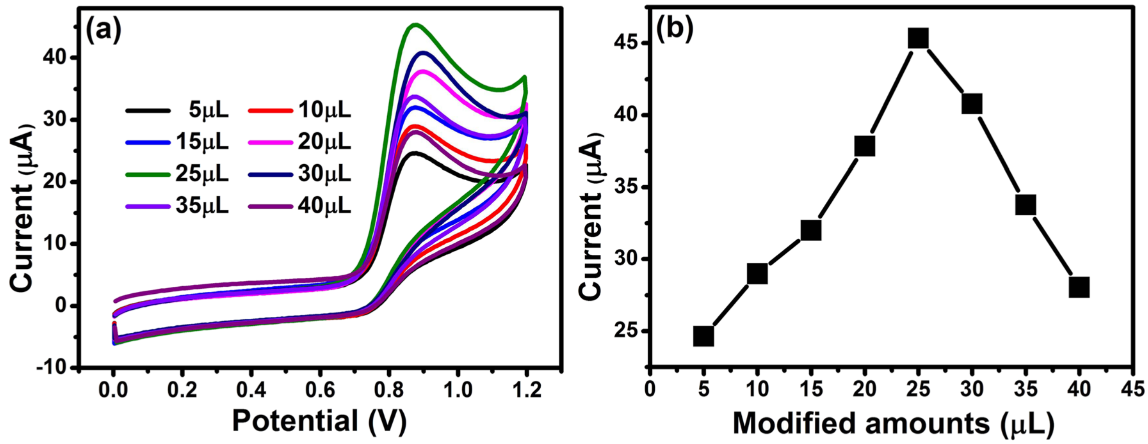

Fig. 6 **a** CV curves of GCE modified with different amounts of rGO-MoS_2 slurry in 500 μM nitrite. **b** Effect of different amounts of rGO-MoS_2 slurry on peak current in 500 μM nitrite

surface of GCE, the modified electrode surface could not be thoroughly covered by rGO-MoS_2 heterostructures, which will cause insufficient active sites for nitrite catalysis. On the other hand, when excessive of rGO-MoS_2 heterostructures was modified on the electrode, the large amount of rGO-MoS_2 slurry may cause the aggregation, blocking the electron transport. As a result, the optimum content of rGO-MoS_2 heterostructures is about 25 μL, and the subsequent measurements were carried out under this condition. Furthermore, the thickness of the rGO-MoS_2 layer was characterized using SEM. As shown in Fig. S1(a, b), the bare GCE is uniformly covered by the rGO-MoS_2 heterostructures. Figure S1(c) reveals the cross-section image of rGO-MoS_2 heterostructures, and the thickness of rGO-MoS_2 slurry is approximately 60 μm on the surface of GCE.

To compare the electrocatalytic activity of the as-prepared electrodes (GCE, rGO/GCE, MoS_2/GCE, and rGO-MoS_2/GCE) towards nitrite detection, the electrochemical properties of the as-prepared electrodes were studied by cyclic voltammograms (CVs) in the potential range of 0.0–1.2 V at a scan rate of 50 mV s^{-1} (vs. Ag/AgCl). Figure 7a illustrates the CVs of as-prepared electrodes in 0.1 M PBS (pH = 7.0) towards 500 μM nitrite. For the bare GCE, a broad oxidation peak appears at the potential of ~0.90 V with a peak current of ~17.3 μA. For the rGO/GCE electrode, a significant oxidation peak response can be observed at ~0.81 V with current about 33.2 μA, which indicates a certain catalytic property on rGO in this current potential window. A higher oxidation current peak (~38.1 μA) can be achieved for MoS_2/GCE comparing with GCE and rGO/GCE but with a higher catalytic potential of ~0.95 V. Moreover, it can be clearly observed that the measured oxidation peak current value can reach to 45.0 μA for rGO-MoS_2/GCE with the potential of ~0.85 V, and the highest catalytic current and more negative potential (than MoS_2/GCE) of rGO-MoS_2 hybrid structures suggest a better catalytic ability towards nitrite than rGO and MoS_2. The results obtained demonstrate that the introduction of rGO can improve the electronic transmission rate as well as increase the surface area to

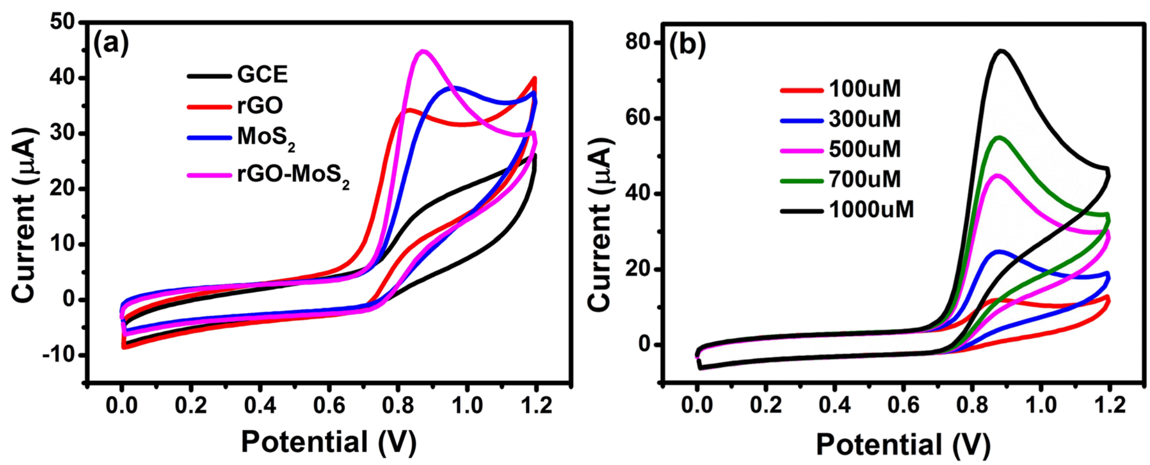

Fig. 7 **a** CV curves of the as-prepared electrodes in 0.1 M PBS (pH = 7.0) with 500 μM nitrite. **b** CV curves of the rGO-MoS_2/GCE electrode in 0.1 M PBS (pH = 7.0) under different concentrations of nitrite: 100, 300, 500, 700, and 1000 μM (scan rate: 50 mV s^{-1})

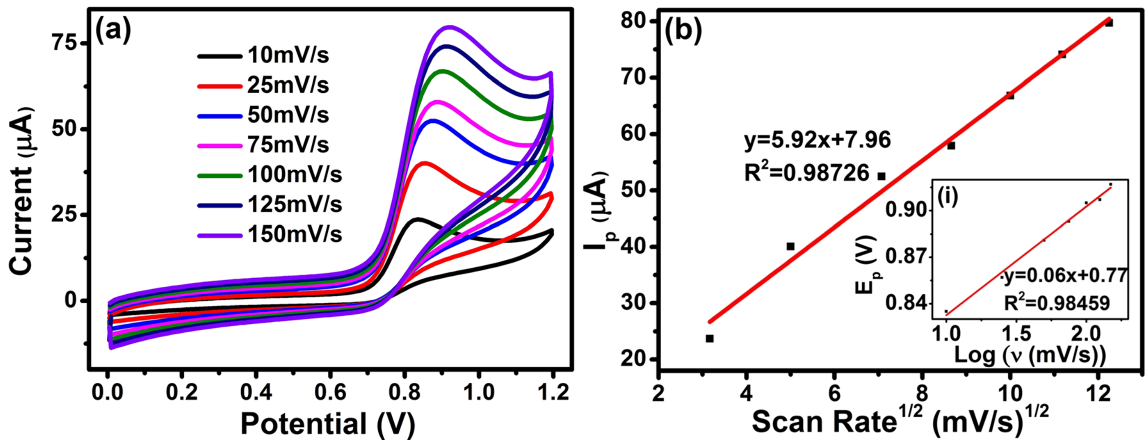

Fig. 8 **a** CV curves of rGO-MoS_2/GCE at different scan rates in 500 μM nitrite. **b** The calibration curve of the peak current vs. the square root of the scan rate (inset image: the peak potential and logarithm of the scan rate (log ν))

capture a large amount of analytes, which consequently can efficiently promote the electro-oxidation of NO_2^-.

Meanwhile, the sensing properties of rGO-MoS_2 heterostructures were further studied by detecting different concentrations of NO_2^-, as shown in Fig. 7b. The measured results demonstrated that the oxidation peak current value proportionally increases with the increasing concentration of NO_2^- from 100 to 1000 μM, which confirmed that the rGO-MoS_2/GCE could effectively determine the different concentrations of NO_2^- in current conditions. As a result, the rGO-MoS_2 heterostructures have shown excellent electrocatalytic properties, which confirmed that the rGO-MoS_2 is indeed a very promising sensing electrode material for the electrochemical NO_2^- sensor.

On the present rGO-MoS_2 electrode, the nitrite could be oxidized at a suitable potential in the PBS solution. As reported by Guidelli et al., the nitrite oxidation is a second-order homogeneous disproportionation process [34]. Thus, the mechanism and overall reaction can be explained with the following process (Eqs. (1–2)):

$$NO_2^- - e^- \rightarrow NO_2 \qquad (1)$$

$$2NO_2 + H_2O \rightarrow NO_2^- + NO_3^- + 2H^+ \qquad (2)$$

From Eqs. (1–2), NO_3^- is the only plausible final product.

The influence of the scan rate on the cyclic voltammetric performance for the rGO-MoS_2/GCE was also carried out in 0.1 M PBS (pH = 7.0) with 500 μM nitrite. Figure 8a depicts the CV responses of rGO-MoS_2/GCE at the presence of 500 μM nitrite at the different scan rates of 10, 25, 50, 75, 100, 125, and 150 mV/s, respectively. The results show that oxidation peak current (I_p) increases linearly with the increasing of the square root of the scan rate ($\nu^{1/2}$), indicating the diffusion-controlled electrocatalytic process (Fig. 8b) [35]. Moreover, it can be observed that the peak potential E_p

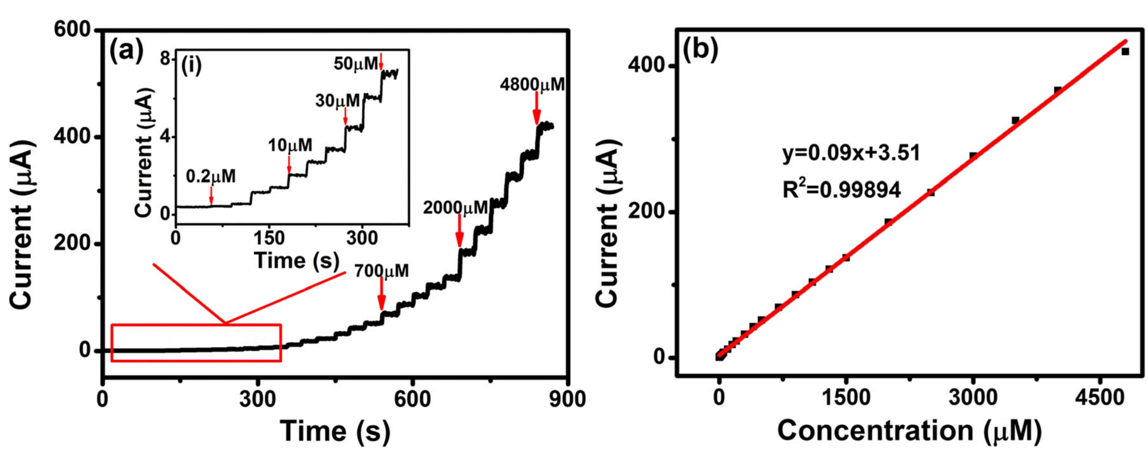

Fig. 9 **a** The amperometric current responses of rGO-MoS_2/GCE for successive addition of nitrite range from 0.2 to 4800 μM in 0.1 M PBS (pH = 7.0) (inset image (*i*): amperometric current response of 0.2 to 50 μM). **b** The linear plot of oxidation current plateau value vs. nitrite concentration

increases with the rising of scan rate, which also exhibited a linear dependence with the logarithm of scan rate (log ν) (Fig. 8b inset). The measured results have clearly demonstrated that the electrocatalytic oxidation process of nitrite is irreversible [36].

Amperometric (i-t) response of rGO-MoS_2/GCE sensor

The amperometric response experiments were also performed on the rGO-MoS_2 heterostructures with stirring rate 200 rpm. Figure 9a shows the stepped amperometric current (i-t) curve of sensor based on rGO-MoS_2/GCE in 0.2 μM–4800 μM nitrite at 0.80 V. And, the inset image illustrates the amplified amperometric current response for the lower nitrite concentration of 0.2–50 μM. The obtained experimental results show that the developed sensor could achieve 95% of the response steady-state value within 3 s after incorporation of a certain nitrite concentration into solution. The outstanding electrochemical properties may be due to the synergistic effect of rGO and MoS_2, which provides fast and efficient electrocatalytic abilities towards nitrite. Meanwhile, the electrochemical performances of rGO-MoS_2/GCE sensor were also studied under the different stirring speeds of the solution [37]. Table S1 (see Supplementary section) illustrates the measured linear range, detection limit, and sensitivity of rGO-MoS_2/GCE sensor, which confirmed that the rGO-MoS_2/GCE sensor exhibits excellent electrochemical properties with stirring rate of 200 rpm. Therefore, the optimum stirring rate is set to be about 200 rpm for the amperometric experiments.

Figure 9b displays the corresponding calibration curve (current (μA) vs. concentration (μM)) of the amperometric response with stirring rate of 200 rpm. The rGO-MoS_2/GCE shows an excellent linear response in the range of 0.2 to 4800 μM. The linear equation of rGO-MoS_2/GCE can be defined as $y = 0.09\times + 3.51$ with a correlation coefficient $R^2 = 0.999$, and the minimum detection limit is estimated to be 0.17 μM under a signal-to-noise ratio (S/N) of 3. Furthermore, to compare the performances of the fabricated rGO-MoS_2/GCE nitrite electrochemical sensor, various nitrite electrochemical sensors based on rGO or MoS_2 sensing materials and non-electrochemical means were summarized in Table 1. Compared with previous works [6, 8–10, 12–14, 16, 38–43], the electrochemical sensor modified with rGO-MoS_2 heterostructures exhibits a very large linear range (0.2 μM–4800 μM) with a detection limit of 0.17 μM, and higher sensitivity (0.46 μA μM^{-1} cm^{-2}) at the potential of 0.8 V. Consequently, it can be concluded that the sensor based on rGO-MoS_2 heterostructures demostrates the best overall response characteristics due to the unique composite nanostructure and synergistic effect, which is promising for nitrite detection.

Table 1 The comparison of sensing characteristics of various nitrite sensors

Sensor material	Determination method	Potential (v)	Linear range (μM)	Detection limit (μM)	Sensitivity (μA·μM^{-1}·cm^{-2})	Reference
CR-GO/GCE	Amperometric	0.8	8.9–167	1	0.0267 A·M^{-1}	[38]
Fe_3O_4/r-GO/GCE	Amperometric	0.7	1–210	0.3	–	[39]
Au-Pd/rGO/GCE	Amperometric	0.85	0.05–1000	0.02	–	[40]
Fe_2O_3/r-GO/GCE	DPV	0.8	0.05–780	0.015	0.204 μA μM^{-1}	[6]
Cu-NDs/rGO/GCE	Amperometric	−0.2	1.25–13,000	0.4	0.214	[12]
Hb/Au/GACS/GCE	Amperometric	0.85	0.05–1000	0.01	0.15	[13]
PANI-MoS_2/GCE	Amperometric	0.9	4.0–4834	1	–	[14]
Fe_3O_4/MoS_2/GCE	Amperometric	0.9	1–2630	0.5	–	[16]
–	FI-luminol CL detection	–	0.008–10	0.002	–	[8]
–	Electrophoresis with fluorescence detection	–	0.002–0.5	0.0006	–	[9]
–	HPLC-CL detection	–	0.002–2.5	0.002	–	[10]
–	FI-gas phase CL detection	–	0.01–10	0.01	–	[41]
–	HPLC-UV (205 nm) detection	–	10 μg/L to 100 μg/mL	10 μg/L	–	[42]
–	FI-UV (312 nm) detection	–	0.03–0.30 μg NO_2^--N/mL	2.9 ng NO_2^--N/mL	–	[43]
rGO-MoS_2/GCE	Amperometric	0.8	0.2–4800	0.17	0.46	This work

DPV differential pulse voltammetry, *HPLC* high-performance liquid chromatography, *CL* chemiluminescence; *FI* flow injection

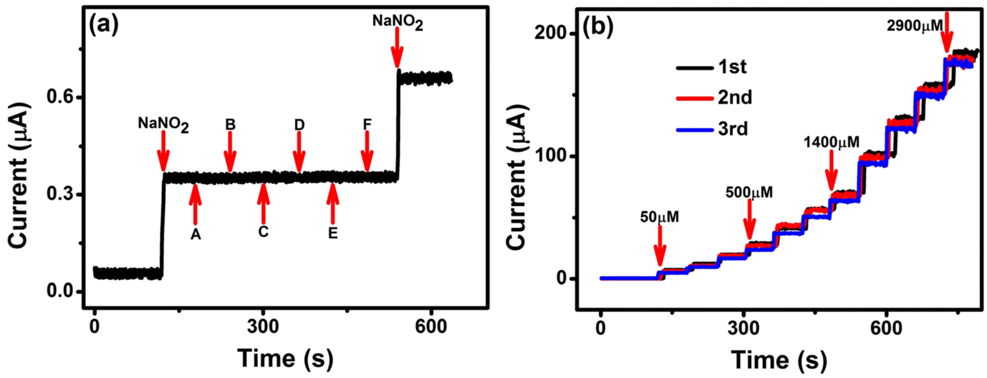

Fig. 10 **a** Interference study of rGO-MoS_2/GCE in the presence of Na_2SO_4 (*A*), KCl (*B*), $NaNO_3$ (*C*), Na_2CO_3 (*D*), glucose (*E*), alcohol (*F*) in 0.1 M PBS (pH = 7.0). **b** Amperometric current responses of three rGO-MoS_2/GCE for successive addition of 50–2900 μM nitrite at the same conditions

Selectivity and reproducibility

To evaluate the selectivity of the as-fabricated sensor towards nitrite, the anti-interference ability of the rGO-MoS_2 heterostructures has also been examined by incorporation of such additives as Na_2SO_4, KCl, $NaNO_3$, Na_2CO_3, glucose, and alcohol into the solution. As shown in Fig. 10a, when nitrite was added, the current increased significantly and reached a steady-state value immediately. However, no apparent amperometric responses were observed when additives were subsequently injected at the regular intervals. Stability of the output sensor's signal suggests that none of the incorporated chemicals have effect on the performance of the sensor in the current conditions. Meanwhile, the reproducibility of the sensor was also determined by detecting the current response with three rGO-MoS_2 modified electrodes, which was prepared using the same method (Fig. 10b). The measured result indicates that the amperometric responses towards the same concentration of nitrite for the different sensors are almost the same. The standard deviation of the sensitivities is calculated to be 0.12, which proves an excellent reproducibility for the developed electrochemical sensor attached with rGO-MoS_2/GCE heterostructures.

Table 2 Determination results of nitrite in the real samples

Sample	Added (μM)	Found (μM)	Recovery (%)
1	50	52.1 ± 3.3	104.2
2	100	105.0 ± 8.1	105.0
3	300	303.1 ± 4.2	101.0
4	500	503.2 ± 3.4	100.6
5	1000	983.8 ± 15.2	98.4
6	1500	1494.3 ± 21.4	99.6
7	2000	1991.8 ± 155.3	99.6
8	2500	2493.3 ± 32.5	99.7
9	3000	2993.2 ± 132.5	99.8
10	3500	3494.4 ± 154.2	99.8
11	4000	3981.2 ± 178.3	99.5

Application to real samples

In order to demonstrate the practicability of the fabricated rGO-MoS_2/GCE sensor, the amperometric response measurements were conducted in known concentrations of nitrite solution. Eleven different concentrations of nitrite samples (50, 100, 300, 500, 1000, 1500, 2000, 2500, 3000, 3500, 4000 μM) were prepared by tap water. Figure S2 (see Supplementary section) exhibits the amperometric responses of the rGO-MoS_2/GCE sensor for the real samples, which indicates that the current can reach a stable value in a relatively short time. Table 2 illustrates the determination results of rGO-MoS_2/GCE sensor under the different nitrite concentrations. The measured recovery values for rGO-MoS_2/GCE sensor vary from 98 to 104%, which confirmed that the fabricated sensor has great potential application nitrite detection in the real samples.

Conclusions

In this work, a simple and facial hydrothermal method for the synthesis of rGO-MoS_2 heterostructures is demonstrated. The electrochemical sensor based on developed rGO-MoS_2 heterostructures was fabricated and used for nitrite measurements. The electrochemical results obtained show that the sensor attached with synthesized rGO-MoS_2 heterostructures can greatly improve the electrocatalytic performance towards the nitrite determination in a solution compared with other sensors based on the conventional solid electrodes. Moreover, the experimental results clearly demonstrated that the fabricated sensor exhibited several advantages including wide linear range (0.2 to 4800 μM); high sensitivity (0.46 $\mu A\ \mu M^{-1}\ cm^{-2}$); low detection limit (0.17 μM); and good selectivity, reproducibility, and availability. The enhanced electrochemical properties of the rGO-MoS_2/GCE sensor can be attributed to the unique hybrid structure sensing electrode and synergistic effect. The as-synthesized rGO-MoS_2 heterostructures can therefore be utilized as promising and unique sensing platform for the development of various nitrite electrochemical devices with enhanced sensing capabilities.

Acknowledgments This work was supported by the National Natural Science Foundation of China (51205274), Higher school science and technology innovation project of Shanxi (2016137, 2016136), Natural Science of Shanxi Province (2016011039, 2014011019-1), Talent project of Shanxi Province (201605D211036), Science and Technology Major Project of the Shan Xi Science and Technology Department (20121101004), and Key Disciplines Construction in Colleges and Universities of Shanxi ([2012]45).

References

1. Yue R, Lu Q, Zhou Y (2011) A novel nitrite biosensor based on single-layer graphene nanoplatelet–protein composite film. Biosens Bioelectron 26:4436–4441. doi:10.1016/j.bios.2011.04.059
2. Zhang D, Ma H, Chen Y, Pang H, Yu Y (2013) Amperometric detection of nitrite based on Dawson-type vanodotungstophosphate and carbon nanotubes. Chim Acta 792:35–44. doi:10.1016/j.aca.2013.07.010
3. Rayman MK, Aris B, Hurst A (1981) Nisin: a possible alternative or adjunct to nitrite in the preservation of meats. Appl Environ Microbiol 41:375–380
4. Dubowski Y, Colussi AJ, Boxe C, Hoffmann MR (2002) Monotonic increase of nitrite yields in the photolysis of nitrate in ice and water between 238 and 294 K. J Phys Chem A 106:6967–6971. doi:10.1021/jp0142942
5. Chen H, Mousty C, Cosnier S, Silveira C, Moura JJG, Almeida MG (2007) Highly sensitive nitrite biosensor based on the electrical wiring of nitrite reductase by [ZnCr-AQS] LDH. Electrochem Commun 9:2240–2245. doi:10.1016/j.elecom.2007.05.030
6. Radhakrishnan S, Krishnamoorthy K, Sekar C, Wilson J, Kim SJ (2014) A highly sensitive electrochemical sensor for nitrite detection based on Fe_2O_3 nanoparticles decorated reduced graphene oxide nanosheets. Appl Catal B 148:22–28. doi:10.1016/j.apcatb.2013.10.044
7. Bru M, Burguete MI, Galindo F, Luis SV, Marin MJ, Vigara L (2006) Cross-linked poly (2-hydroxyethylmethacrylate) films doped with 1, 2-diaminoanthraquinone (DAQ) as efficient materials for the colorimetric sensing of nitric oxide and nitrite anion. Tetrahedron Lett 47:1787–1791. doi:10.1016/j.tetlet.2006.01.030
8. Mikuska P, Vecera Z (2003) Simultaneous determination of nitrite and nitrate in water by chemiluminescent flow-injection analysis. Anal Chim Acta 495:225–232. doi:10.1016/j.aca.2003.08.013
9. Wang X, Adams E, Van Schepdael A (2012) A fast and sensitive method for the determination of nitrite in human plasma by capillary electrophoresis with fluorescence detection. Talanta 97:142–144. doi:10.1016/j.talanta.2012.04.008
10. Kodamatani H, Yamazaki S, Saito K, Tomiyasu T, Komatsu Y (2009) Selective determination method for measurement of nitrite and nitrate in water samples using high-performance liquid chromatography with post-column photochemical reaction and chemiluminescence detection. J Chromatogr A 1216:3163–3167. doi:10.1016/j.chroma.2009.01.096
11. Radhakrishnan S, Sumathi C, Umar A, Kim SJ, Wilson J, Dharuman V (2013) Polypyrrole–poly (3,4-ethylenedioxythiophene)–Ag (PPy–PEDOT–Ag) nanocomposite films for label-free electrochemical DNA sensing. Biosens Bioelectron 47:133–140. doi:10.1016/j.bios.2013.02.049
12. Zhang D, Fang Y, Miao Z, Ma M, Du X, Takahashi S, Anzai J, Chen Q (2013) Direct electrodeposion of reduced graphene oxide and dendritic copper nanoclusters on glassy carbon electrode for electrochemical detection of nitrite. Electrochim Acta 107:656–663. doi:10.1016/j.electacta.2013.06.015
13. Jiang J, Fan W, Du X (2014) Nitrite electrochemical biosensing based on coupled graphene and gold nanoparticles. Biosens Bioelectron 51:343–348. doi:10.1016/j.bios.2013.08.007
14. Zhang Y, Chen P, Wen F, Huang C, Wang H (2016) Construction of polyaniline/molybdenum sulfide nanocomposite: characterization and its electrocatalytic performance on nitrite. Ionics 22:1095–1102. doi:10.1007/s11581-015-1634-5
15. Mutyala S, Mathiyarasu J (2015) Preparation of graphene nanoflakes and its application for detection of hydrazine. Sensors Actuators B Chem 210:692–699. doi:10.1016/j.snb.2015.01.033
16. Zhang Y, Chen P, Wen F, Yuan B, Wang HG (2016) Fe_3O_4 nanospheres on MoS_2 nanoflake: Electrocatalysis and detection of Cr (VI) and nitrite. J Electroanal Chem 761:14–20. doi:10.1016/j.jelechem.2015.12.004
17. Hu R, Gou H, Mo Z, Wei X, Wang Y (2015) Highly selective detection of trace Cu^{2+} based on polyethyleneimine-reduced graphene oxide nanocomposite modified glassy carbon electrode. Ionics 21:3125–3133. doi:10.1007/s11581-015-1499-7
18. Dikin DA, Stankovich S, Zimney EJ, Piner RD, Dommett GH, Evmenenko G, Nguyen ST, Ruoff RS (2007) Preparation and characterization of graphene oxide paper. Nature 448:457–460. doi:10.1038/nature06016
19. Ye J, Chen W, Chen Q, Yu Z, Lee JY (2016) Poly (diallyldimethylammonium chloride)-assisted synthesis of MoS_2/graphene composites with enhanced electrochemical performances for reversible lithium storage. Electrochim Acta 190:538–547. doi:10.1016/j.electacta.2016.01.011
20. Geim AK, Grigorieva IV (2013) Van der Waals heterostructures. Nature 499:419–425. doi:10.1038/nature12385
21. Wang QH, Kalantar-Zadeh K, Kis A, Coleman JN, Strano MS (2012) Electronics and optoelectronics of two-dimensional transition metal dichalcogenides. Nat Nanotechnol 7:699–712. doi:10.1063/1.4852615
22. Huang KJ, Liu YJ, Liu YM, Wang LL (2014) Molybdenum disulfide nanoflower-chitosan-Au nanoparticles composites based electrochemical sensing platform for bisphenol A determination. J Hazard Mater 276:207–215. doi:10.1016/j.jhazmat.2014.05.037
23. Chang K, Chen W, Ma L, Li H, Li H, Huang F, Xu Z, Zhang Q, Lee JY (2011) Graphene-like MoS_2/amorphous carbon composites with high capacity and excellent stability as anode materials for lithium ion batteries. J Mater Chem 21:6251–6257. doi:10.1039/c1jm10174a
24. Loan PTK, Zhang W, Lin CT, Wei KH, Li LJ, Chen CH (2014) Graphene/MoS_2 heterostructures for ultrasensitive detection of DNA hybridisation. Adv Mater 26:4838–4844. doi:10.1002/adma.201401084
25. Patil S, Harle A, Sathaye S, Patil K (2014) Development of a novel method to grow mono-/few-layered MoS_2 films and MoS_2–graphene hybrid films for supercapacitor applications. CrystEngComm 16:10845–10855. doi:10.1039/C4CE01595A
26. Zhang K, Sun H, Hou S (2016) Layered MoS_2–graphene composites for biosensor applications with sensitive electrochemical performance. Anal Methods 8:3780–3787. doi:10.1039/C6AY00959J
27. Hummers WS Jr, Offeman RE (1958) Preparation of graphitic oxide. J Am Chem Soc 80:1339–1339. doi:10.1021/ja01539a017
28. Li H, Yu K, Fu H, Guo BJ, Lei X, Zhu ZQ (2015) MoS_2/graphene hybrid nanoflowers with enhanced electrochemical performances as anode for lithium-ion batteries. J Phys Chem C 119:7959–7968. doi:10.1021/acs.jpcc.5b00890
29. Zhang ZJ, Wang YX, Chou SL, Li HJ, Liu HK, Wang JZ (2015) Rapid synthesis of α-Fe_2O_3/rGO nanocomposites by microwave

autoclave as superior anodes for sodium-ion batteries. J Power Sources 280:107–113. doi:10.1016/j.jpowsour.2015.01.092
30. Chang K, Chen W (2011) L-cysteine-assisted synthesis of layered MoS_2/graphene composites with excellent electrochemical performances for lithium ion batteries. ACS Nano 5:4720–4728. doi:10.1021/nn200659w
31. Li Y, Wang H, Xie L, Liang Y, Hong G, Dai H (2011) MoS_2 nanoparticles grown on graphene: an advanced catalyst for the hydrogen evolution reaction. J Am Chem Soc 133:7296–7299. doi:10.1021/ja201269b
32. Sun Q, Miao H, Hu X, Zhang G, Zhang D, Liu E, Hao Y, Liu X, Fan J (2016) Preparation of MoS_2/RGO nano heterojunction and photoelectric property. J Mater Sci Mater Electron 27:4665–4671. doi:10.1007/s10854-016-4345-4
33. Tan LK, Liu B, Teng JH, Guo S, Low HY, Loh KP (2014) Atomic layer deposition of a MoS_2 film. Nano 6:10584–10588. doi:10.1039/c4nr02451f
34. Guidelli R, Pergola F, Raspi G (1972) Voltammetric behavior of nitrite ion on platinum in neutral and weakly acidic media. Anal Chem 44:745–755. doi:10.1021/ac60312a018
35. Liu L, Cui H, An H, Zhai J, Pan Y (2017) Electrochemical detection of aqueous nitrite based on poly (aniline-co-o-aminophenol)-modified glassy carbon electrode. Ionics 23:1517–1523. doi: 10.1007/s11581-017-1972-6
36. Tau P, Nyokong T (2007) Electrocatalytic activity of arylthio tetrasubstituted oxotitanium (IV) phthalocyanines towards the oxidation of nitrite. Electrochim Acta 52:4547–4553. doi:10.1016/j.electacta.2006.12.059
37. Álvarez-Romero GA, Palomar-Pardavé ME, Ramírez-Silva MT (2007) Development of a novel nitrate-selective composite sensor based on doped polypyrrole. Anal Bioanal Chem 387:1533–1541. doi:10.1007/s00216-006-1021-1
38. Mani V, Periasamy AP, Chen SM (2012) Highly selective amperometric nitrite sensor based on chemically reduced graphene oxide modified electrode. Electrochem Commun 17:75–78. doi:10.1016/j.elecom.2012.02.009
39. Teymourian H, Salimi A, Khezrian S (2013) Fe_3O_4 magnetic nanoparticles/reduced graphene oxide nanosheets as a novel electrochemical and bioeletrochemical sensing platform. Biosens Bioelectron 49:1–8. doi:10.1016/j.bios.2013.04.034
40. Li SS, Hu YY, Wang AJ, Weng X, Chen JR, Feng JJ (2015) Simple synthesis of worm-like Au–Pd nanostructures supported on reduced graphene oxide for highly sensitive detection of nitrite. Sensors Actuators B Chem 208:468–474. doi:10.1016/j.snb.2014.11.056
41. Aoki T, Fukuda S, Hosoi Y, Mukai H (1997) Rapid flow injection analysis method for successive determination of ammonia, nitrite, and nitrate in water by gas-phase chemiluminescence. Anal Chim Acta 349:11–16. doi:10.1016/S0003-2670(97)00273-0
42. Zuo Y, Wang C, Van T (2006) Simultaneous determination of nitrite and nitrate in dew, rain, snow and lake water samples by ion-pair high-performance liquid chromatography. Talanta 70:281–285. doi:10.1016/j.talanta.2006.02.034
43. Burakham R, Oshima M, Grudpan K, Motomizu S (2004) Simple flow-injection system for the simultaneous determination of nitrite and nitrate in water samples. Talanta 64:1259–1265. doi:10.1016/j.talanta.2004.03.059